SUPPORTING INFORMATION

A Close Look at the Structure of the TiO_2-APTES Interface in Hybrid Nanomaterials and at its Degradation Pathway: an Experimental and Theoretical Study

Daniela Meroni[1,2,*], Leonardo Lo Presti[1,3,*], Giovanni Di Liberto[1], Michele Ceotto[1,*], Robert G. Acres[4], Kevin C. Prince[5,6,7], Roberto Bellani[1], Guido Soliveri[8], Silvia Ardizzone[1,2]

[1] *Università degli Studi di Milano, Department of Chemistry, Via Golgi 19, 20133 Milano, Italy*

[2] *Consorzio INSTM, Via Giusti 9, 50121 Firenze, Italy*

[3] *Center for Materials Crystallography, Aarhus University, Langelandsgade 140, DK-8000, Aarhus, Denmark*

[4] *Australian Synchrotron, Imaging and Medical Beamline, Clayton, Victoria, Australia 3168*

[5] *Elettra-Sincrotrone Trieste, 34149 Basovizza, Trieste, Italy*

[6] *Molecular Model Discovery Laboratory, Department of Chemistry and Biotechnology, Swinburne University of Technology, Melbourne, 3122, Australia*

[7] *Istituto Officina dei Materiali, Consiglio Nazionale delle Ricerche,34149 Basovizza, Italy*

[8] *Department of Engineering Physics, Polytechnique Montréal, H3T 1J4 Montreal, Canada*

S1. Technical details

S1.1 Synchrotron measurements and data analysis

The Material Science beamline at Elettra (Basovizza, IT) is equipped with a plane grating monochromator that can tune the photon energy from 22 to 1000 eV, a hemispherical electron energy analyzer (Specs Phoibos 150), and Ar^+ ion sputtering source. During the experiments, the pressure in the main chamber was in the 10^{-9} mbar range and the light spot on the sample was moved after every few scans in order to prevent extended exposure to photons and any resulting radiation damage.

Photoelectron spectroscopy. High-resolution XP spectra were collected in normal emission geometry, using if not otherwise stated a photon energy of 630 eV for O 1s and Ti 2p, 500 eV for N 1s, 350 eV for C 1s, and 150 eV for Si 2p. During measurements with synchrotron light, the light spot on the sample was moved after every few scans in order to prevent extended exposure to photons and any resulting radiation damage. Two to five measurements were carried out for every region, with a spot size of ca. 100 μm in diameter. The spectra were fitted using combined Gaussian−Lorentzian peaks with background correction using the Shirley method. Raw data were normalized to the intensity of the photon beam, measured by means of a high transmission gold mesh. The spectra were fitted using combined Gaussian−Lorentzian peaks with background correction using the Shirley method. Relative elemental contents were estimated by normalizing the peak areas by the corresponding atomic sensitivity factor, in agreement with the relative orientation of the source.[1] Binding energies (B.E.) were corrected for specimen charging by referencing the C-C/C-H component of the C 1s peak to 284.8 eV.

NEXAFS spectroscopy. Nitrogen K-edge and oxygen K-edge NEXAFS spectra were measured at normal (NI, 90°) and grazing (GI, 10°) incidence of the photon beam with respect to the surface. The energy resolution of the N and O NEXAFS is estimated to be 0.3 and 0.8 eV respectively. Polarization of the beam is assumed to be 80-90% linear. Background correction was performed by dividing the C, N signals by the C, N spectra from the fresh substrate. The signals were normalized so that the pre-edge baseline is zero and the post edge intensity is 1.

S1.2 Details of the PAW-DFT calculations

The projector-augmented wave (PAW) potentials were used for the core electron representation.[2] PAW potentials marked with X_h[3] were used for oxygen, carbon, nitrogen and hydrogen, which present very small core radii, to properly reproduce both gas phase and isolated APTES geometries and electronic structure properties (Section S5). The energy cutoff was set at 800 eV. A conjugate-gradient algorithm was employed for geometry optimizations,[4,5] which implied full relaxation of both lattice parameters and coordinates. The potential energy was determined by the full quantum mechanical electronic structure until the differences between two consecutive steps reached the threshold of 10^{-4} eV for total energy and 0.01 eV/Å for the forces. To minimize the self-interaction error, the DFT+U model[6] was employed by setting the U (Hubbard) parameter for 3d orbitals of Titanium equal to 3.3 eV, which is comparable with the values we previously used to study bulk defective titania,[7,8] and to literature values.[9–12] A 21.1 x 11.5 x 25.5 $Å^3$ cell was modeled (Figure S1). Along the **c** direction, a 14 Å-thick vacuum layer was introduced. In this way, the system is fully 3D-periodic, with an infinite number of parallel 2-D slabs separated by a vacuum region thick enough to avoid unphysical interactions between neighboring slabs.

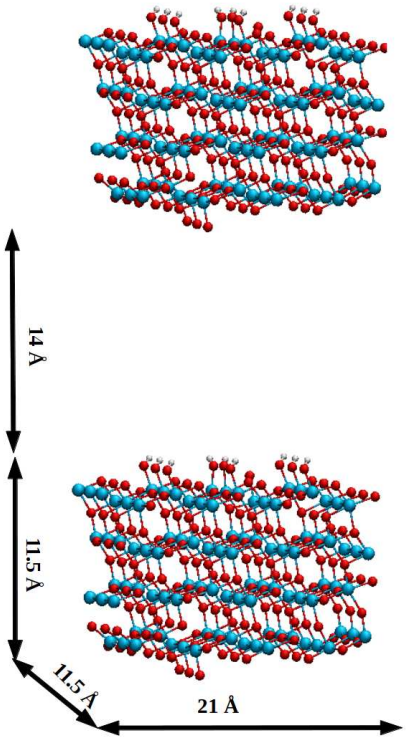

Figure S1. Representation of the computational model for the (101) surface of the anatase polymorph employed in this work. Ti ions are represented as blue spheres, while O and H atoms are drawn in red and white, respectively. Periodic boundary conditions are exploited in three dimensions, but the distance between neighboring slabs makes them independent.

S2. XPS results

Comparing the XPS spectra of the as-synthesized and sputtered TiO_2 layers shows that sputtering removes all surface N species and almost all C species (Figure S2), which clearly indicates their surface contaminant nature as a result of air exposure of the pristine TiO_2 surface. Ti(III) was observed only after sputtering, and its occurrence can be related to the well known preferential sputtering effect of Ar^+ (Figure S3). The O 1s region (Figure 2b, main text) shows a broad signal that is the superposition of several peaks. The O 1s peak is dominated by bulk Ti–O–Ti oxide contributions at 529.9 eV (Table S1). However, the long tail at higher B.E. (binding energy) indicates the presence of other surface species (Figure S4), which might be ascribed to surface hydroxylation and surface C-O contaminants; this latter feature almost disappears after sputtering (Figure S3b).

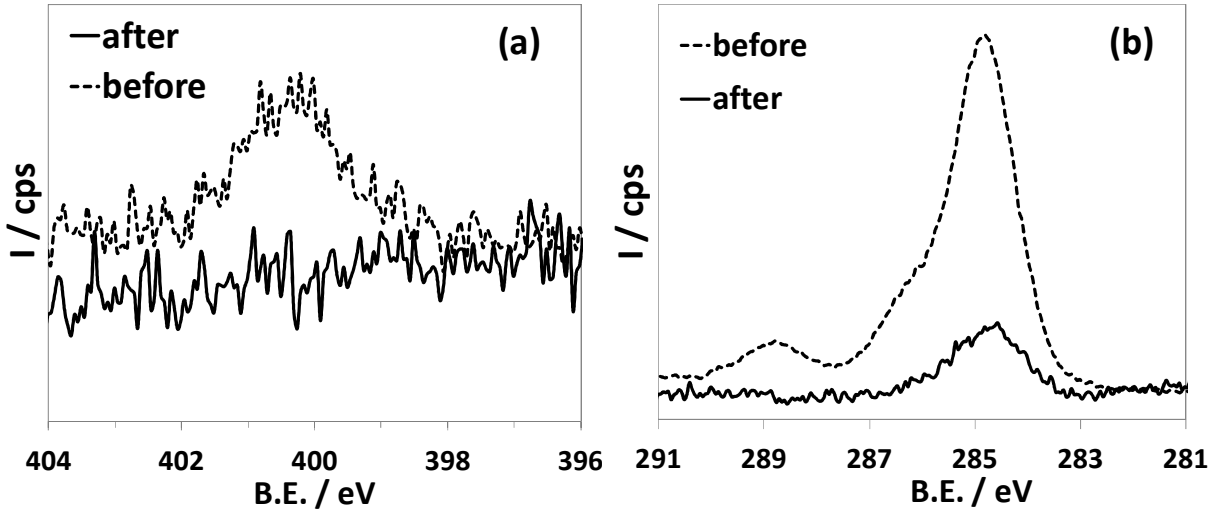

Figure S2. High resolution XP spectra of the unfunctionalized TiO_2 films before (dotted line) and after (full line) sputtering with Ar^+ ions: N 1s (a), C 1s (b).

It is worth noting that the available experimental setup did not allow for an *in situ* irradiation of the samples. Thus, the reference, unfunctionalized sample was irradiated by UV *before* insertion in the XPS chamber, to increase surface hydroxylation as well as to remove surface contaminants (see the main text). However, this procedure did not prevent to still observe a significant surface contamination (see Figure S2 and Table S2), due to the fast adsorption of atmospheric contaminants and the possible occurrence of surface contamination in the XPS chamber itself. The adventitious nature of these contaminants is confirmed by the almost complete disappearance of the N and C signals after sputtering.

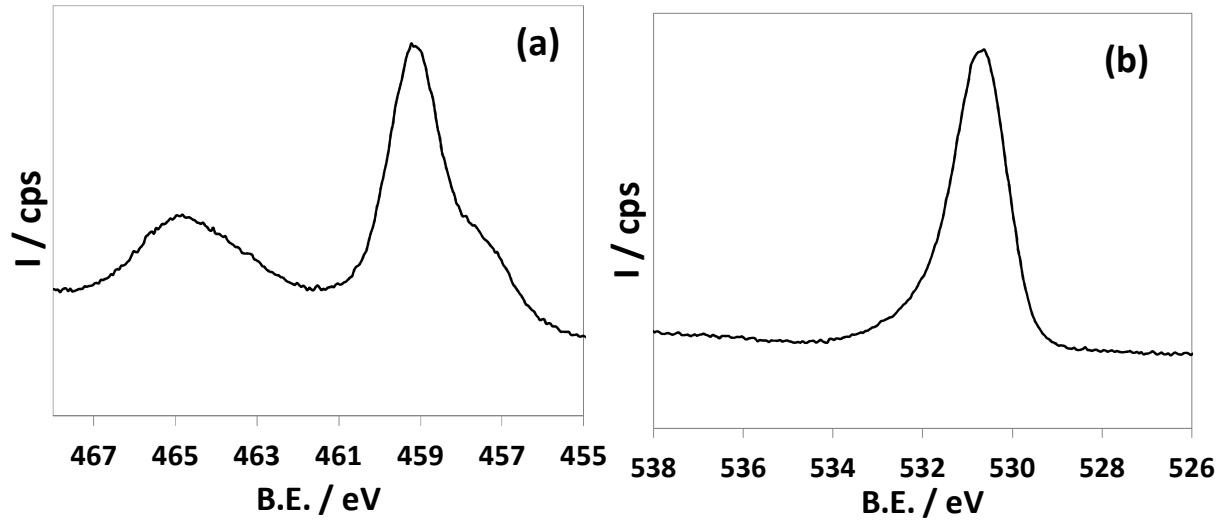

Figure S3. High resolution XP spectra of the unfunctionalized TiO_2 films after sputtering with Ar^+ ions: Ti 2p (a) and O 1s (b).

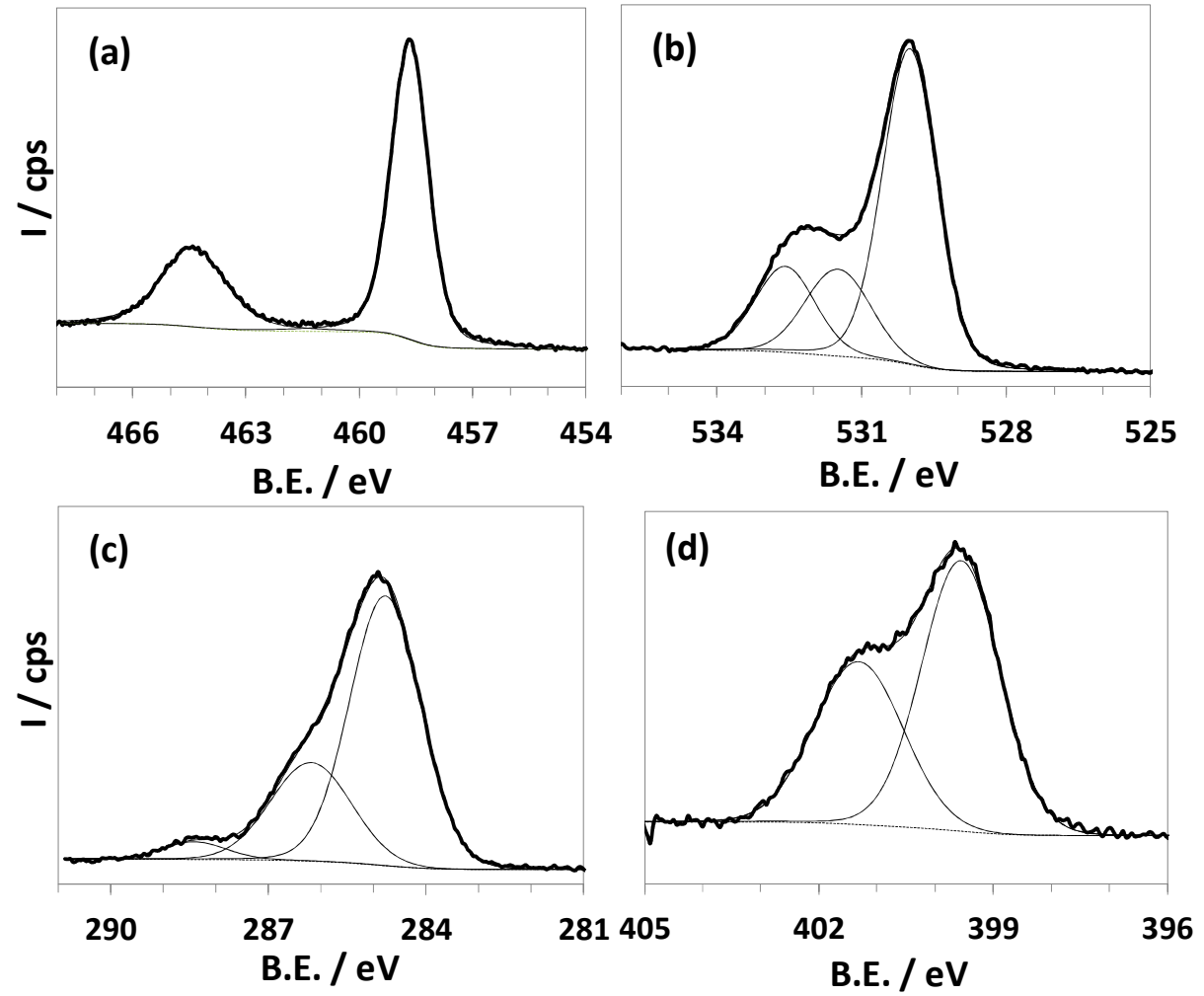

Figure S4. Representative examples of the fitting of high resolution XP spectra (APTES-TiO_2 0 min): Ti 2p (a), O 1s (b), C 1s (c), N 1s (d).

Table S1. Quantification of the O 1s signal in the high resolution XP spectra shown in Figure 3b.

	pristine TiO_2	APTES-TiO_2 0 min	APTES-TiO_2 30 min	APTES-TiO_2 60 min
Position (eV)	529.9	529.7	529.9	529.9
contribution (%)	66	62	51	56
Position (eV)	531.0	531.2	531.2	531.2
contribution (%)	20	19	26	19
Position (eV)	532.2	532.3	532.4	532.4
contribution (%)	14	19	24	26

Table S2. Peak areas, corrected for the intensity of the photon beam and atomic sensitivities, of survey spectra for bare and APTES functionalized TiO_2 films.

	pristine TiO_2	APTES-TiO_2 0 min	APTES-TiO_2 30 min	APTES-TiO_2 60 min
O	$1.79 \cdot 10^5$	$1.97 \cdot 10^5$	$2.37 \cdot 10^5$	$2.57 \cdot 10^5$
Ti	$8.29 \cdot 10^4$	$7.33 \cdot 10^4$	$7.90 \cdot 10^4$	$8.69 \cdot 10^4$
C	$1.86 \cdot 10^5$	$1.63 \cdot 10^5$	$1.27 \cdot 10^5$	$9.64 \cdot 10^4$
N	$8.14 \cdot 10^3$	$3.31 \cdot 10^4$	$1.79 \cdot 10^4$	$1.56 \cdot 10^4$
Si	-	$4.44 \cdot 10^4$	$3.56 \cdot 10^4$	$4.60 \cdot 10^4$

The presence of organic C–O bonds in functionalized samples is also confirmed by inspection at the C 1s region (Figure S5 and Table S3). Although the C 1s region is affected by adventitious carbon, the APTES-functionalized TiO_2 shows a more prominent feature at 286.2 eV with respect to the bare (non-sputtered) sample, which can be related to C-O/C-N bonds. After 60 min of irradiation, the C content indeed decreases from 26% to 19%, (Table S2), whereas the relative weight of the C=O peak at 288.8 eV increases from 7 to 16% (Table S3).

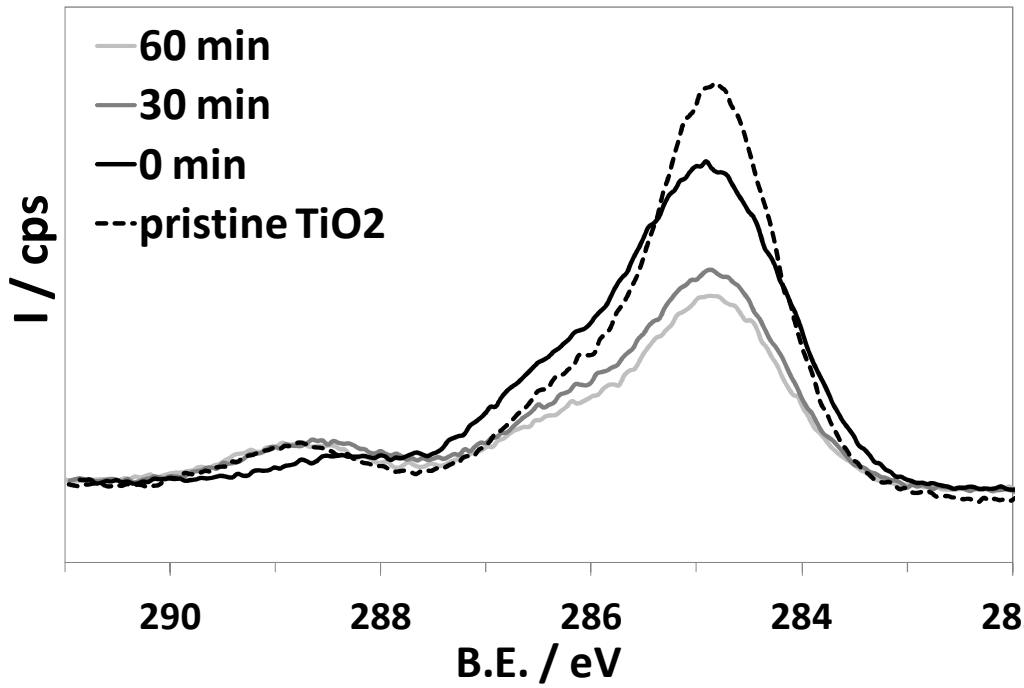

Figure S5. High resolution XP spectra of the pristine (dotted line) and APTES-functionalized TiO_2 (full line) as a function of irradiation time (0, 30, 60 min): C 1 s region.

Table S3. Quantification of the C 1s signal in the high resolution XP spectra shown in Figure S5.

	pristine TiO_2	**APTES-TiO_2 0 min**	**APTES-TiO_2 30 min**	**APTES-TiO_2 60 min**
Position (eV)	284.8	284.8	284.8	284.8
contribution (%)	78	69	66	63
Position (eV)	286.3	286.2	286.2	286.3
contribution (%)	15	28	22	22
Position (eV)	288.8	288.4	288.6	288.8
contribution (%)	7	4	13	16

It is tempting to relate the findings relative to photocatalytic degradation (Figure 3b in the main text) to a complete disappearance of the APTES nitrogen: to confirm this conjecture, we inspected the difference signals obtained after subtracting the bare TiO_2 spectrum (attributed to contaminants) from the structured signals of APTES-containing surfaces (Figure S6). If the amount and chemical nature of contaminants are roughly the same in bare TiO_2 and APTES-functionalized samples, which is a reasonable assumption, difference spectra in Figure S6 should show just the APTES-specific features of the N 1s signal. While this procedure causes peaks II and III to become even sharper at t = 0 min, they essentially disappear in the t = 30, 60 min curves. It is questionable whether peak II could still partly survive in the long tails above 401 eV, as the latter are barely distinguishable from the background noise.

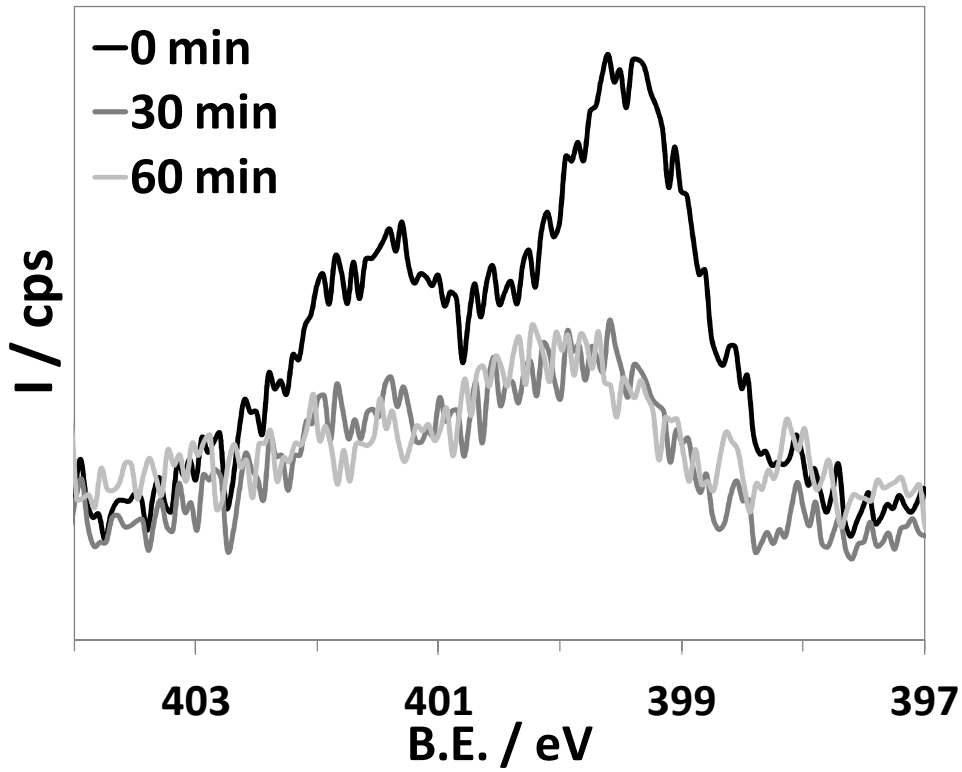

Figure S6. Differential high resolution XP spectra of the N 1s region obtained by subtracting point-by-point the curve of the pristine samples from those of APTES-functionalized TiO_2 at different irradiation times.

S3. FT-IR analysis

The spectrum of the unfunctionalized TiO_2 reference (Figure S7) shows the characteristic bands of the –OH stretching attributable to both free surface hydroxyl groups (3700-3750 cm^{-1}) and hydroxyl groups mutually interacting by hydrogen bonding (broad band at 3700-3000 cm^{-1}). Also the in-plane H-O-H bending mode of undissociated water molecules (~ 1640 cm^{-1}) is visible (Figure S7b). There is no effect of the irradiation time on the observed peaks (Figure S7).

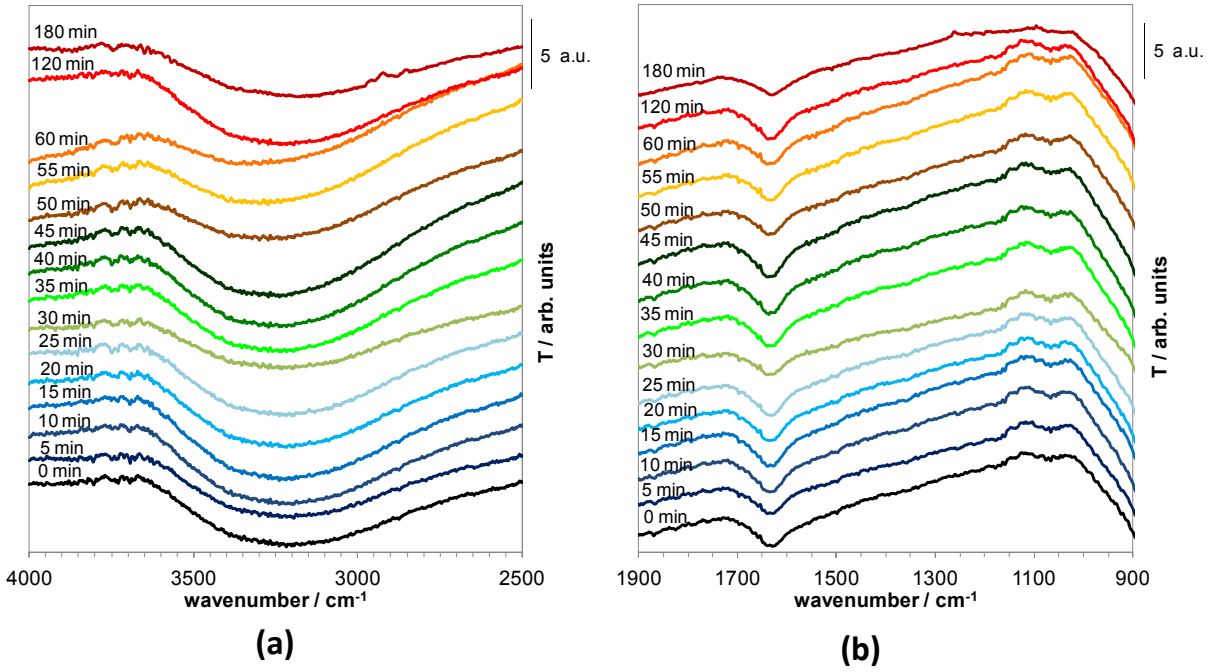

Figure S7. FT-IR spectra of the pristine TiO_2 layer as a function of irradiation time: 4000-2500 cm^{-1} spectral range (a); 1900-900 cm^{-1} spectral range (b).

S4. HR-TEM results

HR-TEM images were collected on an Zeiss Libra FE instrument operating at 200 keV.

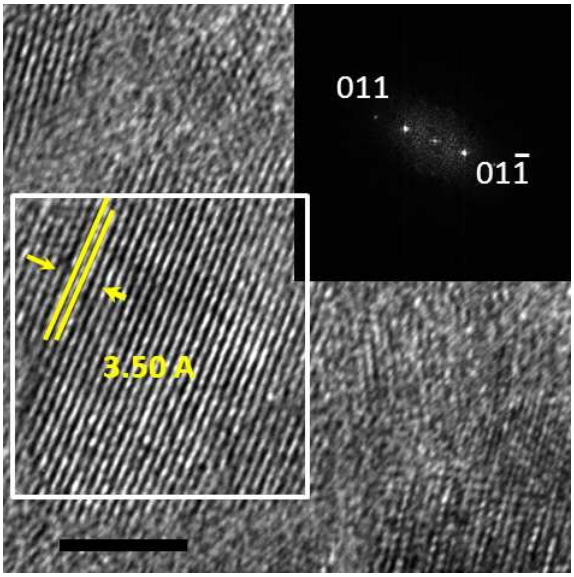

Figure S8. HR-TEM micrograph of the unfunctionalized TiO_2. The highlighted diffraction fringes correspond to {101} facets (in a tetragonal lattice (101) and (011) planes are equivalent by symmetry), as viewed down the [100] direction. The black bar corresponds to a scale of 5 nm. Inset: FFT pattern, with Miller indices of the diffraction spots corresponding to the lattice planes shown in the Figure.

S5. Details on the models employed in PAW-DFT simulations

Isolated (a), (b), (c), (d) molecules, which are attached to TiO_2 in Figure 7 (main text), were optimized with both VASP and NWCHEM packages. Since VASP works with periodic boundary conditions, an infinite lattice of isolated molecules was built by inserting the APTES molecule into a very large cubic primitive cell. In this way, each molecule of the lattice can be assumed not to be influenced by others because of the large intermolecular distance. The lattice parameter of the cubic cell is 30 Å.

We computed the distances matrix on both VASP and NWCHEM optimized structures, where each (ij) element is the distance between the atoms (i) and (j), then we calculated the matrix of the differences, *i.e.* each element of the matrix contains the module of the difference between the computed distance with VASP and NWCHEM, considering the same two atoms. Going further, each element was divided by the computed NWCHEM distance, which was considered the reference value since NWCHEM is more suitable for isolated molecules; in this way, each element of the matrix is the relative deviation from the reference value. Finally, we computed the mean value of this deviations; this value summarizes how much the distances between the atoms are different passing from NWCHEM to VASP. The average mean deviation (AMD) for each molecule is reported in Table S4.

Table S4. Average mean deviation from the reference (NWCHEM) distance values for (a), (b), (c) and (d) molecules. The labels are the same as in Figure 7 in the main text.

Simulated system	**(a)**	**(b)**	**(c)**	**(d)**
AMD %	0.91	0.52	0.23	0.10

We also computed the energy levels distributions for both VASP and NWCHEM results. Figure S9 shows a very good agreement between the two approaches, in particular the HOMO-LUMO gap is very similar in both the different approaches. Furthermore, the energy levels distribution near the HOMO state is quite similar between VASP (black line) and NWCHEM (magenta line). The profiles deep in energy show slight differences; this effect is probably due the pseudopotentials implemented in VASP. In all cases, the HOMO states belong to the nitrogen atom of the amino group.

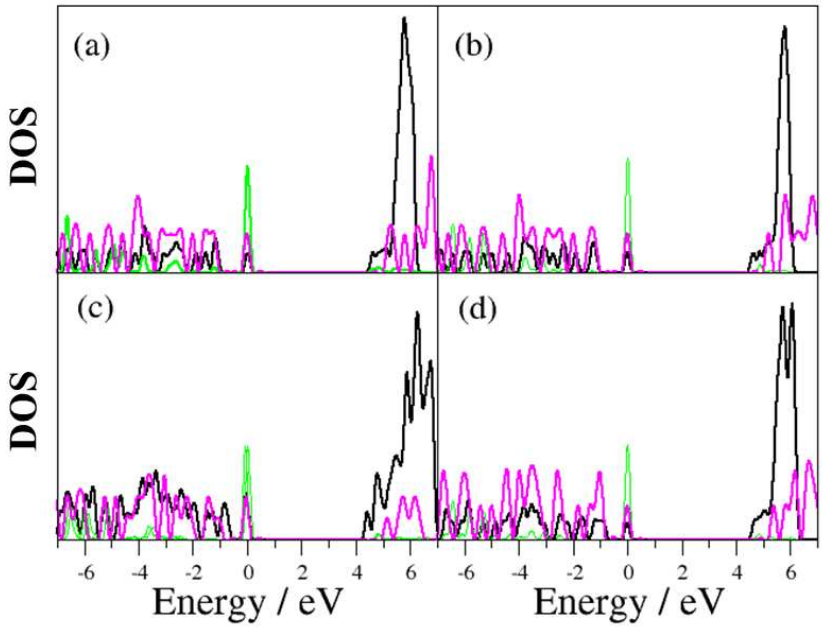

Figure S9. DFT energy levels of the APTES molecules. The (a), (b), (c), (d) labels are the same as in Figure 7. Black line: energy levels distribution computed with VASP; magenta: energy levels distribution computed with NWCHEM; green: energy levels distribution of nitrogen atoms computed with VASP. The zero of energy is set at the HOMO level.

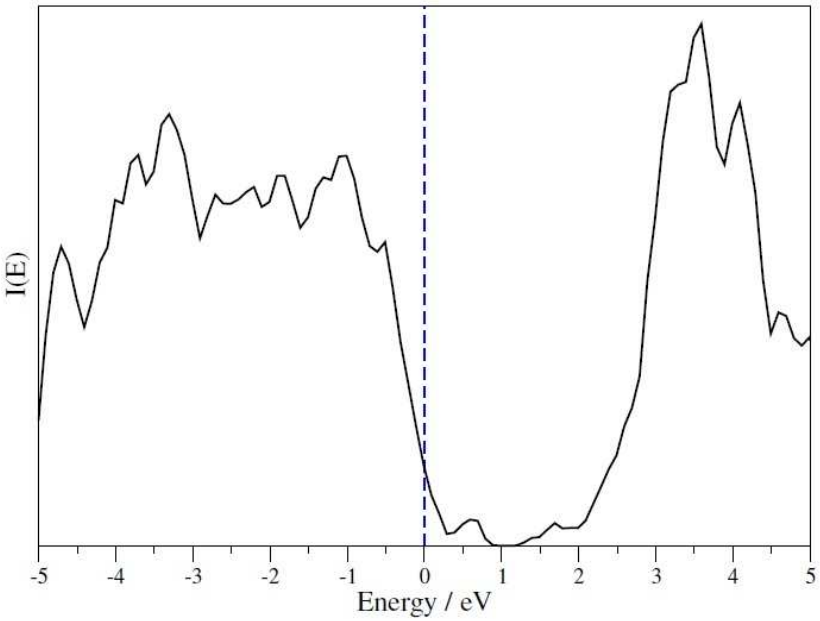

Figure S10. PW-DFT DOS of the fully hydroxylated TiO_2 anatase (101) surface. The vertical blue dashed line represents the Fermi energy. The zero in energy is set equal to the Fermi energy.

REFERENCES

[1] Moulder, J. F.; Stickle, W. F.; Sobol, P. E.; Bomben, K. D. *Handbook of X-ray Photoelectron Spectroscopy*; Chastain, J., ed., Perkin-Elmer Corp.: Eden Prairie, **1992**.

[2] Blöchl, P. E. Projector Augmented-Wave Method. *Phys. Rev. B* **1994**, *50*, 17953–17979.

[3] see https://www.vasp.at/vasp-workshop/slides/pseudoppdatabase.pdf

[4] Teter, M.; Payne, M.; Allan, D. Solution of Schrödinger's Equation for Large Systems. *Phys. Rev. B* **1989**, *40*, 12255–12263.

[5] Bylander, D. M.; Kleinman, L.; Lee, S. Self-consistent Calculations of the Energy Bands and Bonding Properties of B12C3. *Phys. Rev. B* **1990**, *42*, 1394–1403.

[6] Dudarev, S. L.; Botton, G. A.; Savrasov, S. Y.; Humphreys, C. J.; Sutton A. P. Electron-Energy-Loss Spectra and the Structural Stability of Nickel Oxide: An LSDA+U Study. *Phys. Rev. B* **1998**, *57*, 1505-1509.

[7] Marchiori, C.; Di Liberto, G.; Soliveri, G.; Loconte, L.; Lo Presti, L.; Meroni, D.; Ceotto, M.; Oliva, C.; Cappelli, S.; Cappelletti, G.; *et al.* Unraveling the Cooperative Mechanism of Visible-light Absorption in Bulk N,Nb Codoped TiO_2 Powders of Nanomaterials. *J. Phys. Chem. C* **2014**, *118*, 24152–24164.

[8] Rimoldi, L.; Ambrosi, C.; Di Liberto, G.; Lo Presti, L.; Ceotto, M.; Oliva, C.; Meroni, D.; Cappelli, S.; Cappelletti, G.; Soliveri, G.; *et al.* Impregnation versus Bulk Synthesis: How the Synthetic Route Affects the Photocatalytic Efficiency of Nb/Ta:N Codoped TiO_2 Nanomaterials. *J. Phys. Chem. C* **2015**, *119*, 24104−24115.

[9] Finazzi, E.; Di Valentin, C.; Pacchioni, G.; Selloni, A. Excess Electron States in Reduced Bulk Anatase TiO_2: Comparison of Standard GGA, GGA+U, and Hybrid DFT Calculations. *J. Chem. Phys*. **2008**, *129*, 154113.

[10] Morgan, B. J.; Watson, G. W. A DFT + U Description of Oxygen Vacancies at the TiO_2 Rutile (1 1 0) Surface. *Surf. Sci*. **2007**, *601*, 5034–5041.

[11] Mattioli, G.; Filippone, F.; Alippi, P.; Amore Bonapasta, A. Ab Initio Study of the Electronic states Induced by Oxygen Vacancies in Rutile and Anatase TiO_2. *Phys. Rev. B* **2008**, *78*, 241201(R)

[12] Aschauer, U.; He, Y.; Cheng, H.; Li, S.–C.; Diebold, U.; Selloni, A. Influence of Subsurface Defects on the Surface Reactivity of TiO_2: Water on Anatase (101). *J. Phys. Chem. C* **2010**, *114*, 1278–1284.